

# In Pursuit of New Physics with $B_{s,d}^0 \rightarrow \ell^+ \ell^-$

Robert Fleischer <sup>a,b</sup>, Ruben Jaarsma <sup>a</sup> and Gilberto Tetlalmatzi-Xolocotzi <sup>a</sup>

<sup>a</sup>*Nikhef, Science Park 105, NL-1098 XG Amsterdam, Netherlands*

<sup>b</sup>*Department of Physics and Astronomy, Vrije Universiteit Amsterdam,  
NL-1081 HV Amsterdam, Netherlands*

## Abstract

Leptonic rare decays of  $B_{s,d}^0$  mesons offer a powerful tool to search for physics beyond the Standard Model. The  $B_s^0 \rightarrow \mu^+ \mu^-$  decay has been observed at the Large Hadron Collider and the first measurement of the effective lifetime of this channel was presented, in accordance with the Standard Model. On the other hand,  $B_s^0 \rightarrow \tau^+ \tau^-$  and  $B_s^0 \rightarrow e^+ e^-$  have received considerably less attention: while LHCb has recently reported a first upper limit of  $6.8 \times 10^{-3}$  (95% C.L.) for the  $B_s^0 \rightarrow \tau^+ \tau^-$  branching ratio, the upper bound  $2.8 \times 10^{-7}$  (90% C.L.) for the branching ratio of  $B_s^0 \rightarrow e^+ e^-$  was reported by CDF back in 2009. We discuss the current status of the interpretation of the measurement of  $B_s^0 \rightarrow \mu^+ \mu^-$ , and explore the space for New-Physics effects in the other  $B_{s,d}^0 \rightarrow \ell^+ \ell^-$  decays in a scenario with heavy new particles and the feature of Minimal Flavour Violation, including in particular the corresponding version of the MSSM. While the New-Physics effects are strongly suppressed by the ratio  $m_\mu/m_\tau$  of the lepton masses in  $B_s^0 \rightarrow \tau^+ \tau^-$ , they are hugely enhanced by  $m_e/m_\mu$  in  $B_s^0 \rightarrow e^+ e^-$ , and may result in a  $B_s^0 \rightarrow e^+ e^-$  branching ratio about twice as large as the one of  $B_s^0 \rightarrow \mu^+ \mu^-$ , which is about a factor of 50 below the CDF bound; a similar feature arises in  $B_d^0 \rightarrow e^+ e^-$ . Consequently, it would be most interesting to search for the  $B_{s,d}^0 \rightarrow e^+ e^-$  channels at the LHC and Belle II, which may result in an unambiguous signal for physics beyond the Standard Model.



# 1 Introduction

The decay  $B_s^0 \rightarrow \mu^+\mu^-$  belongs to the most interesting processes for testing the flavour sector of the Standard Model (SM). In this framework,  $B_s^0 \rightarrow \mu^+\mu^-$  emerges from quantum loop effects – penguin and box topologies – and is helicity suppressed. Consequently, this channel is strongly suppressed, and in the SM only about three out of one billion  $B_s^0$  mesons decay into the  $\mu^+\mu^-$  final state. Another key feature of the  $B_s^0 \rightarrow \mu^+\mu^-$  decay is that the binding of the anti-bottom quark and the strange quark in the  $B_s^0$  meson is described by a single non-perturbative parameter, the  $B_s^0$ -meson decay constant  $f_{B_s}$  [1]. In scenarios of New Physics (NP),  $B_s^0 \rightarrow \mu^+\mu^-$  may be affected by new particles entering the loop topologies or may even arise at the tree level.

For decades, experiments have searched for the  $B_s^0 \rightarrow \mu^+\mu^-$  decay [2]. It has been a highlight of run 1 of the Large Hadron Collider (LHC) that the  $B_s^0 \rightarrow \mu^+\mu^-$  mode could eventually be observed in a combined analysis by the CMS and LHCb collaborations [3]. The corresponding experimental branching ratio is consistent with the SM prediction.

In addition to the branching ratio,  $B_s^0 \rightarrow \mu^+\mu^-$  offers another observable [4]. It is accessible thanks to the sizeable difference  $\Delta\Gamma_s$  between the decay widths of the  $B_s$  mass eigenstates and is encoded in the effective  $B_s^0 \rightarrow \mu^+\mu^-$  lifetime. The LHCb collaboration has very recently reported a pioneering measurement of this observable, as well as the observation of  $B_s^0 \rightarrow \mu^+\mu^-$  in the analysis of their new data set collected at the ongoing run 2 of the LHC [5].

In the SM, the key difference of  $B_s^0 \rightarrow \mu^+\mu^-$  with respect to  $B_s^0 \rightarrow \tau^+\tau^-$  and  $B_s^0 \rightarrow e^+e^-$  is due to the different lepton masses. In the case of the former decay, the large  $\tau$  mass effectively lifts the helicity suppression, while it gets much stronger for the latter process due to the small electron mass. Consequently, we have SM branching ratios at the  $10^{-6}$  and  $10^{-13}$  level, respectively, while the corresponding  $B_s^0 \rightarrow \mu^+\mu^-$  branching ratio takes a value at the  $10^{-9}$  level [1].

From the experimental point of view, the analysis of  $B_s^0 \rightarrow \tau^+\tau^-$  is challenging because of the reconstruction of the  $\tau$  leptons. Nevertheless, LHCb has recently presented the first upper bound for this channel of  $6.8 \times 10^{-3}$  (95% C.L.) [6]. The  $B_s^0 \rightarrow e^+e^-$  channel has received surprisingly little attention, both from the experimental and theoretical communities, and has so far essentially not played any role in the exploration of flavour physics. The most recent upper bound on the  $B_s^0 \rightarrow e^+e^-$  branching ratio of  $2.8 \times 10^{-7}$  (90% C.L.) was obtained by the CDF collaboration back in 2009 [7]. We have illustrated this situation in Fig. 1.

We will have a fresh look at the search for NP effects with the  $B_s^0 \rightarrow \mu^+\mu^-$  and  $B_d^0 \rightarrow \mu^+\mu^-$  channels in view of the new LHCb data [5], complementing the recent study by Altmannshofer, Niehoff and Straub [8]. However, the main focus of our discussion will be on the  $B_s^0 \rightarrow \tau^+\tau^-$  and  $B_s^0 \rightarrow e^+e^-$  decays (as well as their  $B_d^0$  counterparts), which were not considered in Ref. [8]. The key question is how much space for NP effects is left in these channels by the currently available data, in particular for the experimentally established  $B_s^0 \rightarrow \mu^+\mu^-$  mode.

In order to explore this topic, which is in general very complex, we follow Ref. [8] and consider a framework of NP with the feature of Minimal Flavour Violation (MFV) [9], including the MFV realization of the Minimal Supersymmetric Standard Model (MSSM). We find that the corresponding NP effects are small in  $B_s^0 \rightarrow \tau^+\tau^-$ . However, as the helicity suppression is lifted by new (pseudo)-scalar contributions, we may get a huge enhancement of the branching ratio of  $B_s^0 \rightarrow e^+e^-$  in this scenario, while still

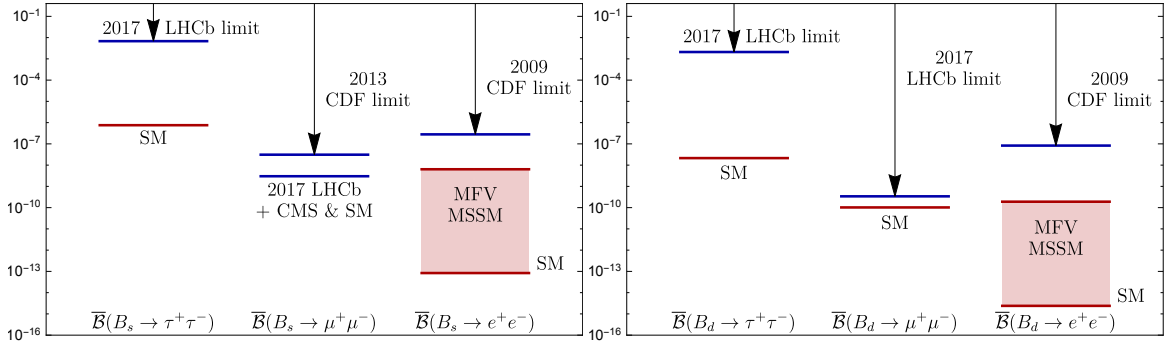


Figure 1: Illustration of the  $B_s^0 \rightarrow \ell^+ \ell^-$  (left panel) and  $B_d^0 \rightarrow \ell^+ \ell^-$  (right panel) branching ratios: current experimental status, SM predictions and the possible enhancement within the MFV MSSM scenario discussed in the text.

having the branching ratio of  $B_s^0 \rightarrow \mu^+ \mu^-$  within the current experimental range. In particular, the branching ratio of  $B_s^0 \rightarrow e^+ e^-$  may be enhanced to about twice the  $B_s^0 \rightarrow \mu^+ \mu^-$  branching ratio, which is a factor of 50 below the CDF limit from 2009. Consequently, it would be most interesting to have a dedicated search for  $B_s^0 \rightarrow e^+ e^-$  and  $B_d^0 \rightarrow e^+ e^-$ , fully exploiting the potential of the LHC, where these decays will be interesting for ATLAS, CMS and LHCb, and the future Belle II experiment at KEK. In view of the theoretical cleanliness of these decays and the possible dramatic enhancement with respect to the SM, we may get an unambiguous signal for New Physics.

In Fig. 2, we have illustrated our analysis of the NP model. The measured branching ratio of the  $B_s^0 \rightarrow \mu^+ \mu^-$  channel allows us to determine an observable  $\overline{R}_{\mu\mu}^s$ , which can be converted into a parameter  $A_{\mu\mu}^s$  characterizing the NP model. The corresponding twofold solutions have very different implications for the branching ratios of the  $B_{s,d}^0 \rightarrow \tau^+ \tau^-$  and  $B_{s,d}^0 \rightarrow e^+ e^-$  channels. The flowchart in Fig. 2 serves as a guideline for the following discussion.

The outline of this paper is as follows: we discuss the theoretical framework for our studies in Section 2. In Section 3, we have a closer look at the state-of-the-art picture following from the experimental results for the  $B_{s,d}^0 \rightarrow \mu^+ \mu^-$  decays, while turning to the  $B_{s,d}^0 \rightarrow \tau^+ \tau^-$  and  $B_{s,d}^0 \rightarrow e^+ e^-$  modes in Sections 4 and 5, respectively. Finally, we summarize our conclusions in Section 6.

## 2 Theoretical Framework

### 2.1 Low-Energy Effective Hamiltonian

Leptonic rare decays of  $\bar{B}_q^0$  mesons ( $q = d, s$ ) are described by the following low-energy effective Hamiltonian [1, 4, 8]:

$$\mathcal{H}_{\text{eff}} = -\frac{G_F}{\sqrt{2}\pi} V_{tq}^* V_{tb} \alpha [C_{10}^{q,\ell\ell} O_{10} + C_S^{q,\ell\ell} O_S + C_P^{q,\ell\ell} O_P + C_{10}^{q,\ell\ell'} O'_{10} + C_S^{q,\ell\ell'} O'_S + C_P^{q,\ell\ell'} O'_P], \quad (1)$$

where  $G_F$  denotes the Fermi constant,  $V_{qq'}$  are elements of the Cabibbo–Kobayashi–Maskawa (CKM) matrix, and  $\alpha$  is the QED fine structure constant. The heavy degrees of freedom have been integrated out and are described by the Wilson coefficients  $C_{10}^{q,\ell\ell'}$ ,  $C_P^{q,\ell\ell'}$  and  $C_S^{q,\ell\ell'}$ , which may depend both on the flavour of the quark  $q$  and on the

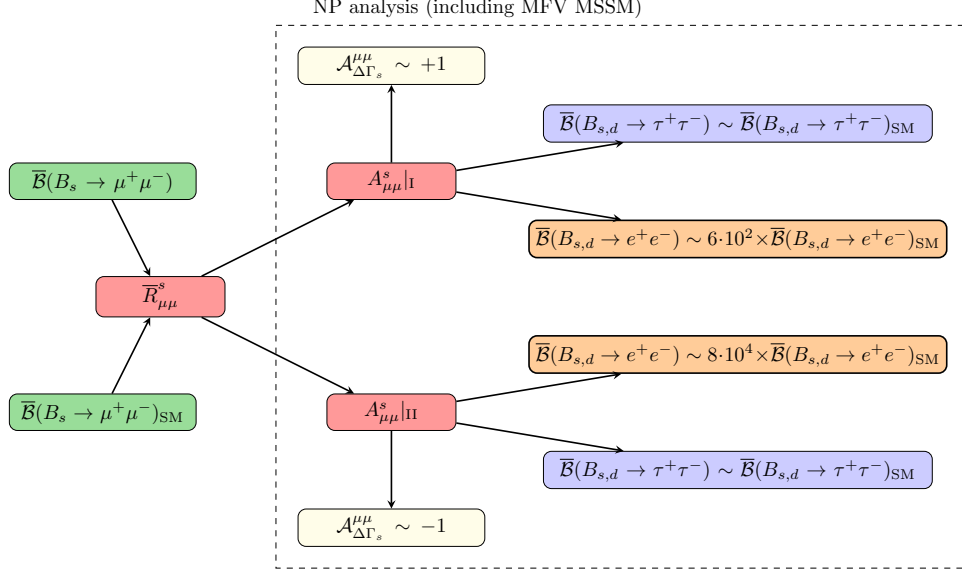


Figure 2: Flowchart illustrating the analysis and interplay of the various  $B_{s,d}^0 \rightarrow \ell^+ \ell^-$  observables within the considered NP model, as discussed in the text.

flavour of the final-state leptons  $\ell^+ \ell^-$ . However, in the SM and NP scenarios with MFV, they are flavour universal.

The Wilson coefficients are associated with the four-fermion operators

$$\begin{aligned} O_{10} &= (\bar{q} \gamma_\mu P_L b) (\bar{\ell} \gamma^\mu \gamma_5 \ell), & O'_{10} &= (\bar{q} \gamma_\mu P_R b) (\bar{\ell} \gamma^\mu \gamma_5 \ell), \\ O_S &= m_b (\bar{q} P_R b) (\bar{\ell} \ell), & O'_S &= m_b (\bar{q} P_L b) (\bar{\ell} \ell), \\ O_P &= m_b (\bar{q} P_R b) (\bar{\ell} \gamma_5 \ell), & O'_P &= m_b (\bar{q} P_L b) (\bar{\ell} \gamma_5 \ell), \end{aligned} \quad (2)$$

where  $m_b$  denotes the  $b$ -quark mass and

$$P_L \equiv \frac{1}{2} (1 - \gamma_5), \quad P_R \equiv \frac{1}{2} (1 + \gamma_5). \quad (3)$$

In the general Hamiltonian in Eq. (1), we have only kept operators which give non-vanishing contributions to  $\bar{B}_q^0 \rightarrow \ell^+ \ell^-$  decays. In the SM, only the  $O_{10}$  operator is present with a real coefficient  $C_{10}^{\text{SM}}$ .

Concerning the impact of NP, the outstanding feature of the  $\bar{B}_q^0 \rightarrow \ell^+ \ell^-$  channels is their sensitivity to (pseudo)-scalar lepton densities entering the operators  $O_{(P)S}$  and  $O'_{(P)S}$ , which have still largely unconstrained Wilson coefficients, thereby offering an interesting avenue for NP effects to enter. The  $\bar{B}_q^0 \rightarrow \ell^+ \ell^-$  decay amplitude has the following structure [1]:

$$A(\bar{B}_q^0 \rightarrow \ell^+ \ell^-) \propto V_{tq}^* V_{tb} f_{B_q} M_{B_q} m_\mu C_{10}^{\text{SM}} [\eta_\lambda P_{\ell\ell}^q + S_{\ell\ell}^q], \quad (4)$$

where  $\lambda = L, R$  describes the helicity of the final-state leptons with  $\eta_L = +1$  and  $\eta_R = -1$ . The quantities

$$P_{\ell\ell}^q \equiv \frac{C_{10}^{q,\ell\ell} - C_{10}^{q,\ell\ell'}}{C_{10}^{\text{SM}}} + \frac{M_{B_q}^2}{2m_\ell} \left( \frac{m_b}{m_b + m_q} \right) \left[ \frac{C_P^{q,\ell\ell} - C_P^{q,\ell\ell'}}{C_{10}^{\text{SM}}} \right] \quad (5)$$

$$S_{\ell\ell}^q \equiv \sqrt{1 - 4 \frac{m_\ell^2}{M_{B_q}^2} \frac{M_{B_q}^2}{2m_\ell} \left( \frac{m_b}{m_b + m_q} \right)} \left[ \frac{C_S^{q,\ell\ell} - C_S^{q,\ell\ell'}}{C_{10}^{\text{SM}}} \right], \quad (6)$$

where  $M_{B_q}$  and  $m_\ell$  are the  $\bar{B}_q^0$  and  $\ell$  masses, respectively, will play a key role in the following discussion. In general, the coefficients  $P_{\ell\ell}^q \equiv |P_{\ell\ell}^q| e^{i\varphi_{P_q}^{\ell\ell}}$  and  $S_{\ell\ell}^q \equiv |S_{\ell\ell}^q| e^{i\varphi_{S_q}^{\ell\ell}}$  have CP-violating phases  $\varphi_{P_q}^{\ell\ell}$  and  $\varphi_{S_q}^{\ell\ell}$ . In the SM, we obtain the simple relations

$$P_{\ell\ell}^q|_{\text{SM}} = 1, \quad S_{\ell\ell}^q|_{\text{SM}} = 0. \quad (7)$$

## 2.2 Decay Observables

The  $B_s^0$  and  $\bar{B}_s^0$  mesons show the phenomenon of  $B_s^0$ – $\bar{B}_s^0$  mixing, which leads to time-dependent decay rates. Experiments actually measure the following time-integrated branching ratio [10]:

$$\bar{\mathcal{B}}(B_s \rightarrow \ell^+ \ell^-) \equiv \frac{1}{2} \int_0^\infty \langle \Gamma(B_s(t) \rightarrow \ell^+ \ell^-) \rangle dt. \quad (8)$$

Here the time-dependent untagged rate, where no distinction is made between initially, i.e. at time  $t = 0$ , present  $B_s^0$  or  $\bar{B}_s^0$  mesons, takes the following form [4, 8, 11]:

$$\begin{aligned} \langle \Gamma(B_s(t) \rightarrow \ell^+ \ell^-) \rangle &\equiv \Gamma(B_s^0(t) \rightarrow \ell^+ \ell^-) + \Gamma(\bar{B}_s^0(t) \rightarrow \ell^+ \ell^-) \\ &= \frac{G_F^2 \alpha^2}{16\pi^3} |V_{ts} V_{tb}^*|^2 f_{B_s}^2 M_{B_s} m_\ell^2 \sqrt{1 - 4 \frac{m_\ell^2}{M_{B_s}^2}} |C_{10}^{\text{SM}}|^2 \\ &\quad \times (|P_{\ell\ell}^s|^2 + |S_{\ell\ell}^s|^2) e^{-t/\tau_{B_s}} [\cosh(y_s t/\tau_{B_s}) + \mathcal{A}_{\Delta\Gamma_s}^{\ell\ell} \sinh(y_s t/\tau_{B_s})], \end{aligned} \quad (9)$$

where the decay width difference  $\Delta\Gamma_s$  enters through the parameter [12]

$$y_s \equiv \frac{\Delta\Gamma_s}{2\Gamma_s} = 0.0645 \pm 0.0045, \quad (10)$$

with  $\tau_{B_s} = 1/\Gamma_s$  denoting the  $B_s^0$  lifetime. Using the quantities introduced above, the observable  $\mathcal{A}_{\Delta\Gamma_s}^{\ell\ell}$  is given as follows [4, 11]:

$$\mathcal{A}_{\Delta\Gamma_s}^{\ell\ell} = \frac{|P_{\ell\ell}^s|^2 \cos(2\varphi_{P_s}^{\ell\ell} - \phi_s^{\text{NP}}) - |S_{\ell\ell}^s|^2 \cos(2\varphi_{S_s}^{\ell\ell} - \phi_s^{\text{NP}})}{|P_{\ell\ell}^s|^2 + |S_{\ell\ell}^s|^2}. \quad (11)$$

Since it is challenging to determine the helicity of the final-state leptons experimentally, the rates in (9) are actually helicity-averaged. The observable  $\mathcal{A}_{\Delta\Gamma_s}^{\ell\ell}$  takes the SM value

$$\mathcal{A}_{\Delta\Gamma_s}^{\ell\ell}|_{\text{SM}} = +1, \quad (12)$$

but is essentially unconstrained when allowing for NP effects [4, 8, 11].

In view of the sizeable  $y_s$ , we have to properly distinguish between the time-integrated branching ratio  $\bar{\mathcal{B}}(B_s \rightarrow \ell^+ \ell^-)$  measured at experiments and the “theoretical” branching ratio  $\mathcal{B}(B_s \rightarrow \ell^+ \ell^-)_{\text{theo}}$ , which corresponds to the decay time  $t = 0$ . These two branching ratios can be converted into each other through the following relation [13]:

$$\mathcal{B}(B_s \rightarrow \ell^+ \ell^-)_{\text{theo}} = \left[ \frac{1 - y_s^2}{1 + \mathcal{A}_{\Delta\Gamma_s}^{\ell\ell} y_s} \right] \bar{\mathcal{B}}(B_s \rightarrow \ell^+ \ell^-). \quad (13)$$

The physics information encoded in the effective lifetime

$$\tau_{\ell\ell}^s \equiv \frac{\int_0^\infty t \langle \Gamma(B_s(t) \rightarrow \ell^+ \ell^-) \rangle dt}{\int_0^\infty \langle \Gamma(B_s(t) \rightarrow \ell^+ \ell^-) \rangle dt} \quad (14)$$

is equivalent to the observable  $\mathcal{A}_{\Delta\Gamma_s}^{\ell\ell}$  [4], which can be determined with the help of

$$\mathcal{A}_{\Delta\Gamma_s}^{\ell\ell} = \frac{1}{y_s} \left[ \frac{(1 - y_s^2) \tau_{\ell\ell}^s - (1 + y_s^2) \tau_{B_s}}{2\tau_{B_s} - (1 - y_s^2) \tau_{\ell\ell}^s} \right]. \quad (15)$$

Moreover,  $\tau_{\ell\ell}^s$  allows us to convert the time-integrated branching ratio determined at experiments into the “theoretical” branching ratio with the help of the relation

$$\mathcal{B}(B_s \rightarrow \ell^+ \ell^-)_{\text{theo}} = \left[ 2 - (1 - y_s^2) \frac{\tau_{\ell\ell}^s}{\tau_{B_s}} \right] \overline{\mathcal{B}}(B_s \rightarrow \ell^+ \ell^-), \quad (16)$$

where all quantities on the right-hand side can be measured [4, 13]. In the case of  $\bar{B}_d^0 \rightarrow \ell^+ \ell^-$  decays,  $y_d$  takes a value at the  $10^{-3}$  level. Consequently, the corresponding observable  $\mathcal{A}_{\Delta\Gamma_d}^{\ell\ell}$  is experimentally not accessible in the foreseeable future.

In order to search for NP effects by means of the branching ratio of the  $B_s^0 \rightarrow \ell^+ \ell^-$  decays, it is useful to introduce the following ratio [4, 11]:

$$\overline{R}_{\ell\ell}^s \equiv \frac{\overline{\mathcal{B}}(B_s \rightarrow \ell^+ \ell^-)}{\overline{\mathcal{B}}(B_s \rightarrow \ell^+ \ell^-)_{\text{SM}}}, \quad (17)$$

which takes by definition the SM value

$$\overline{R}_{\ell\ell}^s|_{\text{SM}} = 1. \quad (18)$$

Using the expressions given above yields

$$\begin{aligned} \overline{R}_{\ell\ell}^s &= \left[ \frac{1 + \mathcal{A}_{\Delta\Gamma_s}^{\ell\ell} y_s}{1 + y_s} \right] (|P_{\ell\ell}^s|^2 + |S_{\ell\ell}^s|^2) \\ &= \left[ \frac{1 + y_s \cos(2\varphi_{P_s}^{\ell\ell} - \phi_s^{\text{NP}})}{1 + y_s} \right] |P_{\ell\ell}|^2 + \left[ \frac{1 - y_s \cos(2\varphi_{S_s}^{\ell\ell} - \phi_s^{\text{NP}})}{1 + y_s} \right] |S_{\ell\ell}|^2, \end{aligned} \quad (19)$$

where  $\phi_s^{\text{NP}}$  denotes a possible NP contribution to the  $B_s^0 - \bar{B}_s^0$  mixing phase

$$\phi_s = -2\beta_s + \phi_s^{\text{NP}}. \quad (20)$$

Current experimental information from  $B_s^0 \rightarrow J/\psi \phi$  and decays with similar dynamics gives the following results [12, 14, 15]:

$$\phi_s = -0.030 \pm 0.033 = -(1.72 \pm 1.89)^\circ \quad (21)$$

$$\phi_s^{\text{NP}} = 0.007 \pm 0.033 = (0.4 \pm 1.9)^\circ, \quad (22)$$

where we have used the SM value  $\phi_s^{\text{SM}} = -2\beta_s = -(2.12 \pm 0.04)^\circ$ . Similar quantities can also be introduced for the  $B_d^0 \rightarrow \ell^+ \ell^-$  decays, in analogy to the expressions given above.

## 2.3 A Scenario for Physics Beyond the Standard Model

A first analysis of the interplay between  $\overline{R}_{\mu\mu}^s$  and  $\mathcal{A}_{\Delta\Gamma_s}^{\mu\mu}$  within specific models of physics beyond the SM was performed in Ref. [11]. In view of the new LHCb results for the  $B_s^0 \rightarrow \mu^+ \mu^-$  mode, a very recent study was performed in Ref. [8], highlighting also the importance of measuring  $\mathcal{A}_{\Delta\Gamma_s}^{\mu\mu}$  for the search and exploration of NP effects. For the following discussion, we shall follow this latter reference and consider an attractive NP scenario as a benchmark which was presented there. It corresponds to models with heavy new degrees of freedom (which are also linearly realized in the electroweak symmetry in the Higgs sector) with the feature of MFV [16]. In particular, also the MFV MSSM falls into this category. This specific model was discussed in detail in Ref. [8], taking also into account the constraints for the Higgs boson and the direct searches of supersymmetric particles at the LHC.

In this scenario, we have universal Wilson coefficients with no new sources of CP violation, where

$$C_{10}^{q,\ell\ell} = C_{10}^{\text{SM}}, \quad C_{10}^{q,\ell\ell'} = 0, \quad C_P^{q,\ell\ell'} = 0, \quad C_S^{q,\ell\ell'} = 0 \quad (23)$$

take values as in the SM, while

$$C_P \equiv C_P^{q,\ell\ell} \quad \text{and} \quad C_S \equiv C_S^{q,\ell\ell} \quad (24)$$

satisfy the relation

$$C_S = -C_P. \quad (25)$$

Consequently, this model is characterized by a single, real NP parameter, yielding

$$P_{\ell\ell}^q \equiv 1 + \frac{M_{B_q}^2}{2m_\ell} \left( \frac{m_b}{m_b + m_q} \right) \left( \frac{C_P}{C_{10}^{\text{SM}}} \right) \quad (26)$$

$$S_{\ell\ell}^q \equiv -\sqrt{1 - 4 \frac{m_\ell^2}{M_{B_q}^2}} \frac{M_{B_q}^2}{2m_\ell} \left( \frac{m_b}{m_b + m_q} \right) \left( \frac{C_P}{C_{10}^{\text{SM}}} \right). \quad (27)$$

Following Ref. [8] and introducing the parameter

$$A_{\ell\ell}^q \equiv 1 - P_{\ell\ell}^q = -\frac{M_{B_q}^2}{2m_\ell} \left( \frac{m_b}{m_b + m_q} \right) \left( \frac{C_P}{C_{10}^{\text{SM}}} \right) \quad (28)$$

gives

$$S_{\ell\ell}^q = \sqrt{1 - 4 \frac{m_\ell^2}{M_{B_q}^2}} A_{\ell\ell}^q. \quad (29)$$

Consequently, we obtain

$$1 = P_{\ell\ell}^q + \frac{S_{\ell\ell}^q}{\sqrt{1 - 4 \frac{m_\ell^2}{M_{B_q}^2}}} \approx P_{\ell\ell}^q + S_{\ell\ell}^q, \quad (30)$$

where the last expression is satisfied with excellent precision for  $\ell = \mu, e$ . It should be noted that within this NP scenario, the parameter

$$\mathcal{A}_q \equiv m_\ell A_{\ell\ell}^q = -\frac{M_{B_q}^2}{2} \left( \frac{m_b}{m_b + m_q} \right) \left( \frac{C_P}{C_{10}^{\text{SM}}} \right) \quad (31)$$



does not depend on the flavour of the final-state leptons  $\ell^+\ell^-$ , showing a tiny dependence on  $q$  through the meson and quark masses.

This model offers an interesting framework to explore NP effects in the  $B_q^0 \rightarrow \tau^+\tau^-$  and  $B_q^0 \rightarrow e^+e^-$  decays. But before focusing on these modes, let us first discuss the picture for the  $B_q^0 \rightarrow \mu^+\mu^-$  channels following from the current data.

Parameter	Value	Unit	Reference
$m_e$	$0.5109989461(31) \times 10^{-3}$	GeV	[17]
$m_\mu$	$105.6583745(24) \times 10^{-3}$	GeV	[17]
$m_\tau$	$1.77686(12)$	GeV	[18]
$m_d$	$(4.7_{-0.4}^{+0.5}) \times 10^{-3}$	GeV	[18]
$m_s$	$0.096_{-0.004}^{+0.008}$	GeV	[18]
$m_b$	$4.18_{-0.03}^{+0.04}$	GeV	[18]
$f_{B_s}$	$(228.4 \pm 3.7) \times 10^{-3}$	GeV	[19]
$f_{B_d}$	$(192.0 \pm 4.3) \times 10^{-3}$	GeV	[19]
$f_{B_s}/f_{B_d}$	$1.201 \pm 0.016$		[19]
$\hat{B}_{B_d}$	$1.26 \pm 0.09$		[19]
$\hat{B}_{B_s}$	$1.32 \pm 0.06$		[19]
$\tau_{B_s}$	$1.505 \pm 0.005$	ps	[12]
$\tau_{B_d}$	$1.520 \pm 0.004$	ps	[12]
$M_{B_s}$	$5.36682(22)$	GeV	[18]
$M_{B_d}$	$5.27962(15)$	GeV	[18]
$y_s$	$0.0645 \pm 0.0045$		[12]
$\Delta M_s$	$17.757 \pm 0.021$	ps $^{-1}$	[12]
$\Delta M_d$	$0.5064 \pm 0.0019$	ps $^{-1}$	[12]
$\phi_s$	$-0.030 \pm 0.033$		[12]
$ V_{td} $	$0.008575_{-0.000098}^{+0.000076}$		[15]
$ V_{ts} $	$0.04108_{-0.00057}^{+0.00030}$		[15]
$ V_{tb} $	$0.999119_{-0.000012}^{+0.000024}$		[15]
$\lambda$	$0.22509_{-0.00028}^{+0.00029}$		[15]
$\beta_s$	$0.01852_{-0.00032}^{+0.00032}$		[15]

Table 1: Input parameters used in the numerical evaluations of this paper.

### 3 The Decays $B_s^0 \rightarrow \mu^+\mu^-$ and $B_d^0 \rightarrow \mu^+\mu^-$

#### 3.1 Experimental Status

Using the results of Ref. [1] and rescaling them to the updated parameters collected in Table 1, we obtain the following SM branching ratios:

$$\overline{\mathcal{B}}(B_s \rightarrow \mu^+\mu^-)_{\text{SM}} = (3.57 \pm 0.16) \times 10^{-9} \quad (32)$$

$$\overline{\mathcal{B}}(B_d \rightarrow \mu^+\mu^-)_{\text{SM}} = (1.02 \pm 0.06) \times 10^{-10}. \quad (33)$$

On the experimental side, the LHCb collaboration has recently presented updated measurements of the  $B_s^0 \rightarrow \mu^+\mu^-$  and  $B_d^0 \rightarrow \mu^+\mu^-$  branching ratios [5]:

$$\overline{\mathcal{B}}(B_s \rightarrow \mu^+\mu^-)_{\text{LHCb'17}} = (3.0 \pm 0.6_{-0.2}^{+0.3}) \times 10^{-9} \quad (34)$$

$$\overline{\mathcal{B}}(B_d \rightarrow \mu^+ \mu^-)_{\text{LHCb}'17} = (1.5^{+1.2+0.2}_{-1.0-0.1}) \times 10^{-10}. \quad (35)$$

The CP-averaged signal for  $B_s^0 \rightarrow \mu^+ \mu^-$  has a statistical significance of  $7.8\sigma$ , while  $B_d^0 \rightarrow \mu^+ \mu^-$  has a significance of  $1.6\sigma$ , corresponding to  $\overline{\mathcal{B}}(B_d \rightarrow \mu^+ \mu^-) < 3.4 \times 10^{-10}$  (95% C.L.). These experimental results are consistent with the SM predictions within the uncertainties. In 2013, the CMS collaboration reported the following result [20]:

$$\overline{\mathcal{B}}(B_s \rightarrow \mu^+ \mu^-)_{\text{CMS}'13} = (3.0^{+1.0}_{-0.9}) \times 10^{-9}, \quad (36)$$

which corresponds to a signal with  $4.3\sigma$  significance. The ATLAS collaboration presented the constraint  $\overline{\mathcal{B}}(B_s \rightarrow \mu^+ \mu^-)_{\text{ATLAS}'16} = (0.9^{+1.1}_{-0.8}) \times 10^{-9}$  in 2016 [21], which we give for comparison. The combination of the results in Eqs. (34) and (36) gives

$$\overline{\mathcal{B}}(B_s \rightarrow \mu^+ \mu^-)_{\text{LHCb}'17+\text{CMS}} = (3.0 \pm 0.5) \times 10^{-9}, \quad (37)$$

where we have calculated the average by applying the procedure of the Particle Data Group (PDG) [18].

The LHCb collaboration has very recently reported a first measurement of the effective lifetime of the  $B_s^0 \rightarrow \mu^+ \mu^-$  decay [5]:

$$\tau_{\mu\mu}^s = [2.04 \pm 0.44(\text{stat}) \pm 0.05(\text{syst})] \text{ ps}. \quad (38)$$

Using the expression

$$\frac{\tau_{\mu\mu}^s}{\tau_{B_s}} = \frac{1 + 2y_s \mathcal{A}_{\Delta\Gamma_s}^{\mu\mu} + y_s^2}{(1 + y_s \mathcal{A}_{\Delta\Gamma_s}^{\ell\ell})(1 - y_s^2)}, \quad (39)$$

with Eq. (12) and the numerical inputs in Table 1, we obtain the SM prediction

$$\tau_{\mu\mu}^s|_{\text{SM}} = \frac{\tau_{B_s}}{1 - y_s} = (1.61 \pm 0.01) \text{ ps}. \quad (40)$$

It agrees with the LHCb value, although the experimental uncertainties are too large to draw further conclusions. Using Eq. (15), we may convert Eq. (38) into

$$\mathcal{A}_{\Delta\Gamma_s}^{\mu\mu} = 8.24 \pm 10.72, \quad (41)$$

where the error is fully dominated by the huge uncertainty on the effective lifetime  $\tau_{\mu\mu}^s$ . As we have the model-independent relation

$$-1 \leq \mathcal{A}_{\Delta\Gamma_s}^{\mu\mu} \leq +1, \quad (42)$$

it will be crucial to improve the experimental precision for this observable in the future data taking at the LHC.

### 3.2 General Constraints on New Physics

Let us first have a look at the  $B_s^0 \rightarrow \mu^+ \mu^-$  decay observables. Using Eqs. (32) and (37), we can determine the ratio  $\overline{R}_{\mu\mu}^s$  from Eq. (17):

$$\overline{R}_{\mu\mu}^s|_{\text{LHCb}'17+\text{CMS}} = 0.84 \pm 0.16. \quad (43)$$

Assuming that we have no new CP-violating phases in  $P_{\mu\mu}^s$  and  $S_{\mu\mu}^s$ , as in the NP model introduced in Subsection 2.3, expression (19) reduces to

$$\overline{R}_{\mu\mu}^s = \left[ \frac{1 + y_s \cos \phi_s^{\text{NP}}}{1 + y_s} \right] |P_{\mu\mu}^s|^2 + \left[ \frac{1 - y_s \cos \phi_s^{\text{NP}}}{1 + y_s} \right] |S_{\mu\mu}^s|^2. \quad (44)$$

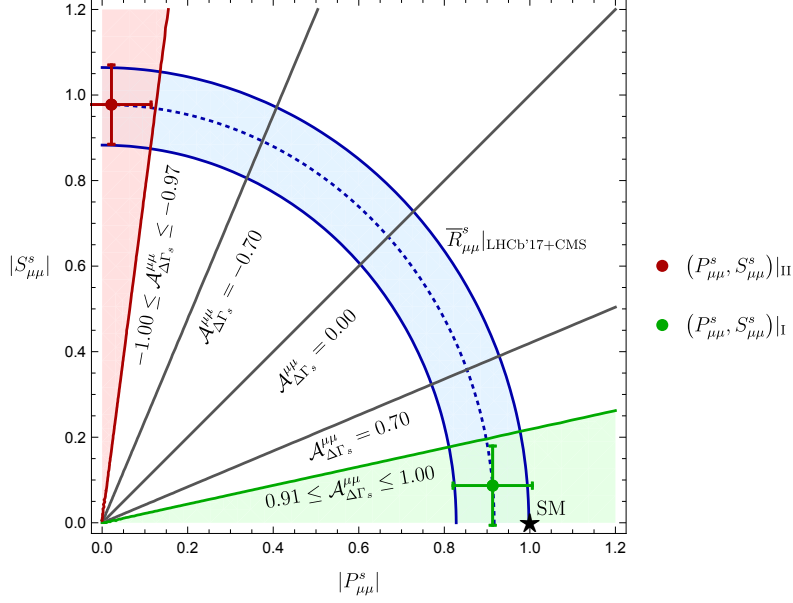


Figure 3: Constraints in the  $|P_{\mu\mu}^s|$ - $|S_{\mu\mu}^s|$  plane following from  $\bar{R}_{\mu\mu}^s$ , shown as the blue circular band. A measurement of the effective lifetime  $\tau_{\mu\mu}^s$  and thus  $\mathcal{A}_{\Delta\Gamma_s}^{\mu\mu}$  pins down values for  $|P_{\mu\mu}^s|$  and  $|S_{\mu\mu}^s|$ , as illustrated by the grey lines, assuming trivial CP-violating NP phases  $\varphi_{P_s}^{\mu\mu}, \varphi_{S_s}^{\mu\mu} \in \{0, \pi\}$ . The data points with error bars correspond to the situation arising in the NP scenario introduced in Subsection 2.3, see Eq. (69) and the corresponding discussion.

Using the experimental value of  $\phi_s^{\text{NP}}$  in Eq. (21) we get

$$\cos \phi_s^{\text{NP}} = 1.0000(2), \quad (45)$$

which allows us to convert Eq. (43) into a circular band in the  $|P_{\mu\mu}^s|$ - $|S_{\mu\mu}^s|$  plane, as shown in Fig. 3. The experimental picture of  $\phi_s^{\text{NP}}$  is fully consistent with the NP scenario introduced in Subsection 2.3. The observable  $\mathcal{A}_{\Delta\Gamma_s}^{\mu\mu}$  provides another constraint in this parameter space. Assuming real coefficients  $P_{\mu\mu}^s$  and  $S_{\mu\mu}^s$ , Eq. (11) yields

$$\mathcal{A}_{\Delta\Gamma_s}^{\mu\mu} = \cos \phi_s^{\text{NP}} \left[ \frac{|P_{\mu\mu}^s|^2 - |S_{\mu\mu}^s|^2}{|P_{\mu\mu}^s|^2 + |S_{\mu\mu}^s|^2} \right], \quad (46)$$

fixing a straight line in the  $|P_{\mu\mu}^s|$ - $|S_{\mu\mu}^s|$  plane through the measured value of  $\mathcal{A}_{\Delta\Gamma_s}^{\mu\mu}$ , as illustrated by the grey contours in Fig. 3 for a variety of assumed values of this observable. Consequently,  $\bar{R}_{\mu\mu}^s$  and  $\mathcal{A}_{\Delta\Gamma_s}^{\mu\mu}$  allow us to determine  $|P_{\mu\mu}^s|$  and  $|S_{\mu\mu}^s|$ , which can be accomplished with the help of the following expressions:

$$|P_{\mu\mu}^s| = \sqrt{\frac{(1 + y_s)(\cos \phi_s^{\text{NP}} + \mathcal{A}_{\Delta\Gamma_s}^{\mu\mu})\bar{R}_{\mu\mu}^s}{(1 + y_s \cos \phi_s^{\text{NP}})(\cos \phi_s^{\text{NP}} + \mathcal{A}_{\Delta\Gamma_s}^{\mu\mu}) + (1 - y_s \cos \phi_s^{\text{NP}})(\cos \phi_s^{\text{NP}} - \mathcal{A}_{\Delta\Gamma_s}^{\mu\mu})}} \quad (47)$$

$$|S_{\mu\mu}^s| = \sqrt{\frac{(1 + y_s)(\cos \phi_s^{\text{NP}} - \mathcal{A}_{\Delta\Gamma_s}^{\mu\mu})\bar{R}_{\mu\mu}^s}{(1 + y_s \cos \phi_s^{\text{NP}})(\cos \phi_s^{\text{NP}} + \mathcal{A}_{\Delta\Gamma_s}^{\mu\mu}) + (1 - y_s \cos \phi_s^{\text{NP}})(\cos \phi_s^{\text{NP}} - \mathcal{A}_{\Delta\Gamma_s}^{\mu\mu})}}. \quad (48)$$

Interestingly, as the NP phases enter as  $2\varphi_{P_s}^{\mu\mu}$  and  $2\varphi_{S_s}^{\mu\mu}$  in Eqs. (11) and (19), we cannot reveal minus signs of  $P_{\mu\mu}^s$  and  $S_{\mu\mu}^s$ , which correspond to  $\varphi_{P_s}^{\mu\mu}, \varphi_{S_s}^{\mu\mu} = \pi$ , leading

to terms of  $2\pi$  in the arguments of the relevant trigonometric functions, thereby leaving them unchanged.

In order to test the SM with the  $B_d^0 \rightarrow \mu^+\mu^-$  decay it is advantageous to consider the ratio of its branching ratio and the one of  $B_s^0 \rightarrow \mu^+\mu^-$  [22]. We obtain the following general expression:

$$\begin{aligned} \frac{\overline{\mathcal{B}}(B_d \rightarrow \mu^+\mu^-)}{\overline{\mathcal{B}}(B_s \rightarrow \mu^+\mu^-)} &= \frac{\tau_{B_d}}{\tau_{B_s}} \left[ \frac{1 - y_s^2}{1 - y_d^2} \right] \left[ \frac{1 + \mathcal{A}_{\Delta\Gamma_d}^{\mu\mu} y_d}{1 + \mathcal{A}_{\Delta\Gamma_s}^{\mu\mu} y_s} \right] \left[ \frac{|P_{\mu\mu}^d|^2 + |S_{\mu\mu}^d|^2}{|P_{\mu\mu}^s|^2 + |S_{\mu\mu}^s|^2} \right] \times \\ &\times \frac{M_{B_d}}{M_{B_s}} \sqrt{\frac{1 - 4(m_\mu^2/M_{B_d}^2)}{1 - 4(m_\mu^2/M_{B_s}^2)}} \left( \frac{f_{B_d}}{f_{B_s}} \right)^2 \left| \frac{V_{td}}{V_{ts}} \right|^2. \end{aligned} \quad (49)$$

The CKM factor  $|V_{td}/V_{ts}|$  is required to utilize this ratio and has to be determined in a way that is robust with respect to the impact of NP effects. Assuming the unitarity of the CKM matrix, it can be extracted from the the length

$$R_t \equiv \sqrt{(1 - \bar{\rho})^2 + \bar{\eta}^2} = \frac{1}{\lambda} \left| \frac{V_{td}}{V_{cb}} \right| \quad (50)$$

of the Unitarity Triangle (UT) as  $|V_{cb}| = |V_{ts}| + \mathcal{O}(\lambda^2)$ . Here  $\lambda \equiv |V_{us}|$  is the Wolfenstein parameter [23], and  $(\bar{\rho}, \bar{\eta})$  describes the apex of the UT in the complex plane [24]. Taking subleading corrections in  $\lambda$  into account and employing the UT side

$$R_b \equiv \sqrt{\bar{\rho}^2 + \bar{\eta}^2} = \left( 1 - \frac{\lambda^2}{2} \right) \frac{1}{\lambda} \left| \frac{V_{ub}}{V_{cb}} \right|, \quad (51)$$

we obtain

$$\left| \frac{V_{td}}{V_{ts}} \right| = \lambda \left[ \frac{\sqrt{(1 - R_b \cos \gamma)^2 + (R_b \sin \gamma)^2}}{1 - 1/2(1 - 2R_b \cos \gamma)\lambda^2} \right] + \mathcal{O}(\lambda^5), \quad (52)$$

where  $\gamma$  is the angle between  $R_b$  and the real axis.

Using pure tree decays of the kind  $B \rightarrow D^{(*)}K^{(*)}$  [25, 26],  $\gamma$  can be determined in a theoretically clean way (for an overview, see [27]). The current experimental value is given as follows [15]:

$$\gamma = (72.1_{-5.8}^{+5.4})^\circ. \quad (53)$$

In the future, thanks to Belle II [28] and the LHCb upgrade [29], the uncertainty is expected to be reduced to the  $1^\circ$  level.

Concerning the  $R_b$  side, it can be determined with the help of  $|V_{ub}|$  and  $|V_{cb}|$  extracted from analyses of exclusive and inclusive semileptonic  $B$  decays (for an overview, see the corresponding review in Ref. [18]). The current status can be summarized as

$$R_b|_{\text{incl}} = 0.46 \pm 0.03, \quad R_b|_{\text{excl}} = 0.41 \pm 0.02, \quad (54)$$

with the average

$$R_b = 0.44 \pm 0.04. \quad (55)$$

The determinations of  $\gamma$  and  $R_b$  using pure tree decays are very robust with respect to NP effects. Consequently, they allow us to determine the ratio in Eq. (52) in a way

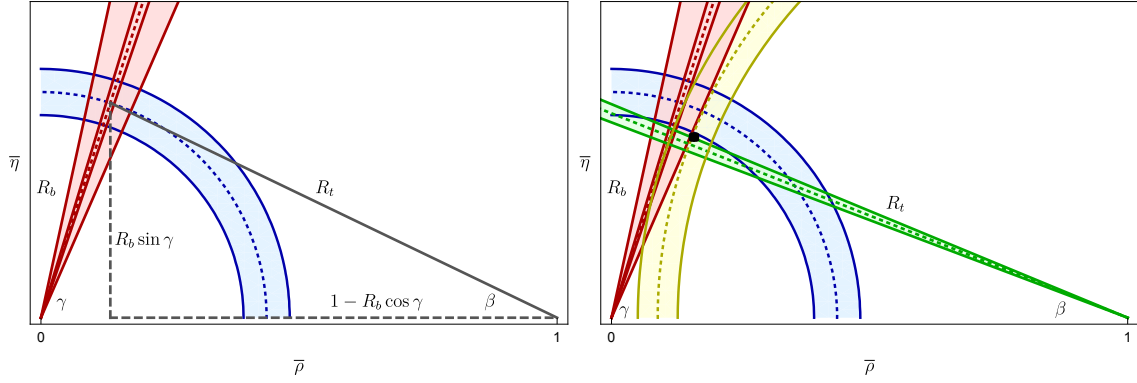


Figure 4: Illustration of the UT in the complex plane. The left panel illustrates the determination of the side  $R_t$ , where the blue circular band for  $R_b$  corresponds to the average in Eq. (55) and the wide red sector to the current value of  $\gamma$  in Eq. (53); the narrow red sector illustrates the future improvement to  $1^\circ$  precision. In the right panel, we add constraints from  $\Delta M_s/\Delta M_d$  and CP violation in  $B_d^0 \rightarrow J/\psi K_S$ , and show the small black region for the apex following from the comprehensive analysis of Ref. [15].

that is also very robust concerning NP contributions, serving as the reference value for the analysis of Eq. (49). The current data with the average value of  $R_b$  in Eq. (55) give

$$\left| \frac{V_{td}}{V_{ts}} \right| = 0.220 \pm 0.010, \quad (56)$$

where the error may be reduced to 0.002 in the Belle II and LHCb upgrade era. We have illustrated the resulting situation for the UT in the complex plane in the left panel of Fig. 4. Thanks to the specific shape of the UT, we observe that the uncertainty of  $R_t$  is fully governed by  $\gamma$ , while the uncertainty of  $R_b$  has a minor impact. Consequently, also the discrepancy between the inclusive and exclusive determinations in Eq. (54) has fortunately a negligible effect in this case. It is impressive to see the impact of the future extraction of  $\gamma$ , allowing a very precise determination of  $R_t$ . For completeness, in the right panel of Fig. 4, we show other constraints in the  $\bar{\rho}$ - $\bar{\eta}$  plane following from  $\Delta M_s/\Delta M_d$  and the determination of the CKM angle  $\beta = (21.6 \pm 0.9)^\circ$  through CP violation in  $B_d^0 \rightarrow J/\psi K_S^0$  decays, taking penguin effects into account [14]. For more comprehensive analyses of the UT, the reader is referred to Refs. [15, 30, 31].

Using the CKM factor  $|V_{td}/V_{ts}|$  as determined through Eq. (52), we may convert the measured ratio of the  $B_{s,d}^0 \rightarrow \mu^+ \mu^-$  branching ratios into the following parameter:

$$U_{\mu\mu}^{ds} \equiv \sqrt{\frac{|P_{\mu\mu}^d|^2 + |S_{\mu\mu}^d|^2}{|P_{\mu\mu}^s|^2 + |S_{\mu\mu}^s|^2}} = \left[ \frac{\tau_{B_s}}{\tau_{B_d}} \left[ \frac{1 - y_d^2}{1 - y_s^2} \right] \left[ \frac{1 + \mathcal{A}_{\Delta\Gamma_s}^{\mu\mu} y_s}{1 + \mathcal{A}_{\Delta\Gamma_d}^{\mu\mu} y_d} \right] \frac{M_{B_s}}{M_{B_d}} \sqrt{\frac{1 - 4(m_\mu^2/M_{B_s}^2)}{1 - 4(m_\mu^2/M_{B_d}^2)}} \right] \times \left( \frac{f_{B_s}}{f_{B_d}} \right)^2 \left| \frac{V_{ts}}{V_{td}} \right|^2 \left[ \frac{\overline{\mathcal{B}}(B_d^0 \rightarrow \mu^+ \mu^-)}{\overline{\mathcal{B}}(B_s^0 \rightarrow \mu^+ \mu^-)} \right]^{1/2}, \quad (57)$$

which satisfies

$$U_{\mu\mu}^{ds}|_{\text{SM}} = 1. \quad (58)$$

For NP models with MFV, which are characterized by universal Wilson coefficients, we have – with excellent accuracy – also a value of  $U_{\mu\mu}^{ds}$  around one. A tiny difference may

arise from the following small differences [18]:

$$M_{B_s} - M_{B_d} = (0.0872 \pm 0.0003) \text{ GeV}$$

$$\frac{m_b}{m_b + m_d} - \frac{m_b}{m_b + m_s} = 0.021 \pm 0.002. \quad (59)$$

We shall return to this parameter in the next Subsection (see Eq. (74)).

The current data give

$$U_{\mu\mu}^{ds} = 1.26 \pm 0.49, \quad (60)$$

where the error is unfortunately too large to draw conclusions. At the end of the LHCb upgrade, corresponding to  $50 \text{ fb}^{-1}$  of integrated luminosity, LHCb expects to determine the ratio  $\overline{\mathcal{B}}(B_d^0 \rightarrow \mu^+ \mu^-) / \overline{\mathcal{B}}(B_s^0 \rightarrow \mu^+ \mu^-)$  with a precision at the 35% level [29]. Assuming a measurement of  $\tau_{\mu\mu}^s$ , which enters in  $\mathcal{A}_{\Delta\Gamma_s}^{\mu\mu}$  through Eq. (15), with a precision of 5% [4] and a reduction in the uncertainty of  $\gamma$  to  $1^\circ$  would yield

$$U_{\mu\mu}^{ds} = 1.26 \pm 0.23, \quad (61)$$

which would still not allow a stringent test in view of the significant uncertainty. We can straightforwardly generalize the observable  $U_{\mu\mu}^{ds}$  defined in Eq. (57) to neutral  $B_{d,s}^0$  decays with  $\tau^+ \tau^-$  and  $e^+ e^-$  leptons in the final state.

Should future measurements find a result for  $U_{\mu\mu}^{ds}$  consistent with 1, thereby supporting the picture of MFV, we could extract the  $SU(3)$ -breaking ratio of “bag” parameters describing  $B_q^0 - \bar{B}_q^0$  mixing (see also Ref. [32]):

$$\frac{\hat{B}_{B_s}}{\hat{B}_{B_d}} = \frac{\tau_{B_s}}{\tau_{B_d}} \left[ \frac{1 - y_d^2}{1 - y_s^2} \right] \left[ \frac{1 + \mathcal{A}_{\Delta\Gamma_s}^{\mu\mu} y_s}{1 + \mathcal{A}_{\Delta\Gamma_d}^{\mu\mu} y_d} \right] \left[ \frac{\overline{\mathcal{B}}(B_d^0 \rightarrow \mu^+ \mu^-)}{\overline{\mathcal{B}}(B_s^0 \rightarrow \mu^+ \mu^-)} \right] \left[ \frac{\Delta M_s}{\Delta M_d} \right], \quad (62)$$

allowing – in principle – an interesting test of lattice QCD. An agreement between experiment and theory would also support the lattice QCD calculation of the decay constants  $f_{B_q}$ , which are key inputs for the SM branching ratios. However, even in the LHCb upgrade era, we would get a precision for Eq. (62) at the level of  $\pm 37\%$ , while current lattice QCD calculations give the following picture [19]:

$$\frac{\hat{B}_{B_s}}{\hat{B}_{B_d}} \Big|_{\text{Lattice}} = 1.05 \pm 0.09. \quad (63)$$

In order to determine the ratio of the “bag” parameters using Eq. (62) with the same relative error as the one achieved by the current lattice calculations in Eq. (63), the measurement of  $\overline{\mathcal{B}}(B_d^0 \rightarrow \mu^+ \mu^-) / \overline{\mathcal{B}}(B_s^0 \rightarrow \mu^+ \mu^-)$  should reach the 6% precision while having the 5% error in the measurement of the effective lifetime as for the LHCb upgrade. In this future scenario, we would be able to achieve a precision of  $\pm 0.06$  for the determination of the observable  $U_{\mu\mu}^{ds}$ .

### 3.3 New Physics Benchmark Scenario

Let us now consider the situation in the NP scenario introduced in Subsection 2.3. Using (28) and (29) for the expression of  $\overline{R}_{\mu\mu}^s$  in (44), we obtain

$$\overline{R}_{\mu\mu}^s = \left[ \frac{1 + y_s \cos \phi_s^{\text{NP}}}{1 + y_s} \right] \left( 1 - 2A_{\mu\mu}^s \right) + \frac{2}{1 + y_s} \left[ 1 - 2 \frac{m_\mu^2}{M_{B_s}^2} \left( 1 - y_s \cos \phi_s^{\text{NP}} \right) \right] (A_{\mu\mu}^s)^2, \quad (64)$$

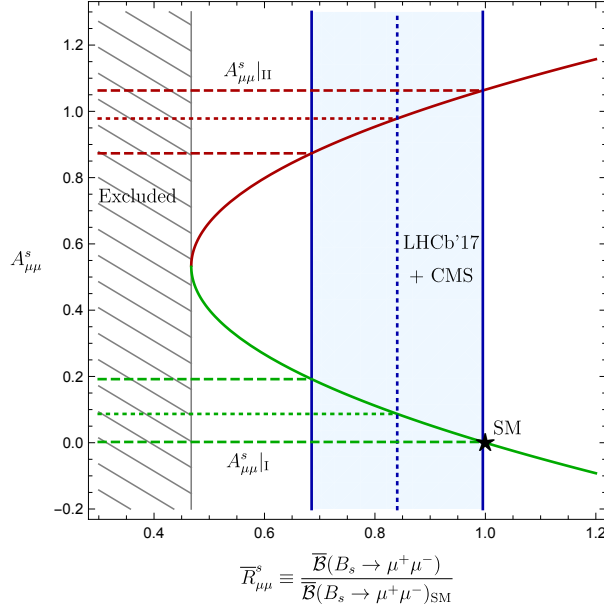


Figure 5: Determination of the NP parameter  $A_{\mu\mu}^s$  from the observable  $\bar{R}_{\mu\mu}^s$ .

which allows us to determine the NP parameter

$$A_{\mu\mu}^s = \frac{1}{2} \left[ \frac{1 + y_s \cos \phi_s^{\text{NP}} \pm \sqrt{\chi_{\mu\mu}^s}}{1 - 2 \frac{m_\mu^2}{M_{B_s}^2} (1 - y_s \cos \phi_s^{\text{NP}})} \right], \quad (65)$$

where the argument of the square root is given by

$$\begin{aligned} \chi_{\mu\mu}^s \equiv & 2(1 + y_s) \bar{R}_{\mu\mu}^s - (1 - y_s \cos \phi_s^{\text{NP}}) \left[ 1 + y_s \cos \phi_s^{\text{NP}} \right. \\ & \left. + 4 \frac{m_\mu^2}{M_{B_s}^2} \left\{ (1 + y_s) \bar{R}_{\mu\mu}^s - (1 + y_s \cos \phi_s^{\text{NP}}) \right\} \right]. \end{aligned} \quad (66)$$

It is interesting to note that real solutions require

$$\chi_{\mu\mu}^s \geq 0, \quad (67)$$

which implies the following lower bound (see also Refs. [11, 33]):

$$\bar{R}_{\mu\mu}^s \geq \frac{1 - y_s}{2} \left[ 1 - 2 \frac{m_\mu^2}{M_{B_s}^2} - 2 y_s \frac{m_\mu^2}{M_{B_s}^2} + \dots \right] = 0.47. \quad (68)$$

In Fig. 5, where the current experimental range for  $\bar{R}_{\mu\mu}^s$  is shown through the blue vertical band, we have illustrated this situation, and obtain the twofold solution

$$A_{\mu\mu}^s|_{\text{I}} = 0.09 \pm 0.09 \quad , \quad A_{\mu\mu}^s|_{\text{II}} = 0.98 \pm 0.09. \quad (69)$$

Using Eqs. (5) and (6) together with our previous results for  $A_{\mu\mu}^s$ , we obtain

$$\begin{aligned} (P_{\mu\mu}^s, S_{\mu\mu}^s)|_{\text{I}} &= (0.91 \pm 0.09, 0.09 \pm 0.09) \\ (P_{\mu\mu}^s, S_{\mu\mu}^s)|_{\text{II}} &= (0.02 \pm 0.09, 0.98 \pm 0.09). \end{aligned} \quad (70)$$

In Fig. 3, we have shown these solutions as the data points with error bars to illustrate the current situation in the NP scenario.

Interestingly,  $\bar{R}_{\mu\mu}^s$  takes a value in the regime of the SM for  $A_{\mu\mu}^s \sim 0$  and  $A_{\mu\mu}^s \sim 1$ . As was pointed out in Ref. [8], these cases – and the twofold solution for  $A_{\mu\mu}^s$  in general – can be resolved through a measurement of the observable

$$\mathcal{A}_{\Delta\Gamma_s}^{\mu\mu} = \cos\phi_s^{\text{NP}} \left[ \frac{1 - 2A_{\mu\mu}^s + 4\frac{m_\mu^2}{M_{B_s}^2}(A_{\mu\mu}^s)^2}{1 - 2A_{\mu\mu}^s + 2(A_{\mu\mu}^s)^2\left(1 - 2\frac{m_\mu^2}{M_{B_s}^2}\right)} \right] = \frac{1 - 2A_{\mu\mu}^s}{1 - 2A_{\mu\mu}^s + 2(A_{\mu\mu}^s)^2}. \quad (71)$$

Here we have used Eq. (45) and neglected the tiny ratios of masses  $m_\mu^2/M_{B_s}^2 = 0.0004$  in the latter expression. As can be seen in Eq. (71), the cases  $A_{\mu\mu}^s \sim 0$  and  $A_{\mu\mu}^s \sim 1$  correspond to  $\mathcal{A}_{\Delta\Gamma_s}^{\mu\mu} \sim +1$  (as in the SM) and  $\mathcal{A}_{\Delta\Gamma_s}^{\mu\mu} \sim -1$ , respectively. The current experimental picture is consistent with both possibilities. We show  $\mathcal{A}_{\Delta\Gamma_s}^{\mu\mu}$  as a function of  $\bar{R}_{\mu\mu}^s$  in Fig. 6, where we indicate also the  $1\sigma$  region of the measured  $B_s^0 \rightarrow \mu^+\mu^-$  branching ratio in Eq. (37). Using the values for  $A_{\mu\mu}^s$  in Eq. (69) yields

$$\mathcal{A}_{\Delta\Gamma_s}^{\mu\mu}|_{\text{I}} = 0.982(41), \quad \mathcal{A}_{\Delta\Gamma_s}^{\mu\mu}|_{\text{II}} = -0.9990(86). \quad (72)$$

Let us now have a look at the decay  $B_d^0 \rightarrow \mu^+\mu^-$  within this NP scenario. In Fig. 7, we show the correlation between  $\bar{\mathcal{B}}(B_d \rightarrow \mu^+\mu^-)$  and  $\bar{\mathcal{B}}(B_s \rightarrow \mu^+\mu^-)$ . Using the current measurement of the latter branching ratio yields

$$\bar{\mathcal{B}}(B_d \rightarrow \mu^+\mu^-)|_{\text{I}} = (8.6 \pm 1.6) \times 10^{-11}, \quad \bar{\mathcal{B}}(B_d \rightarrow \mu^+\mu^-)|_{\text{II}} = (9.6 \pm 1.8) \times 10^{-11}. \quad (73)$$

Finally, we obtain the following results for the parameter  $U_{\mu\mu}^{ds}$  introduced in Eq. (57):

$$U_{\mu\mu}^{ds}|_{\text{I}} = 1.00095(98), \quad U_{\mu\mu}^{ds}|_{\text{II}} = 0.9892(18). \quad (74)$$

As expected from the discussion in the previous subsection for NP models with MFV, this quantity shows a tiny difference from one due to the mass differences in Eq. (59).

## 4 The Decays $B_s^0 \rightarrow \tau^+\tau^-$ and $B_d^0 \rightarrow \tau^+\tau^-$

### 4.1 Observables

As is evident from Eq. (9), the helicity suppression of the SM rates of the  $B_{s,d}^0 \rightarrow \tau^+\tau^-$  channels is essentially lifted through the large mass of the  $\tau$  leptons. Within the SM, we obtain the following predictions:

$$\bar{\mathcal{B}}(B_s \rightarrow \tau^+\tau^-)_{\text{SM}} = (7.56 \pm 0.35) \times 10^{-7}, \quad (75)$$

$$\bar{\mathcal{B}}(B_d \rightarrow \tau^+\tau^-)_{\text{SM}} = (2.14 \pm 0.12) \times 10^{-8}. \quad (76)$$

In order to calculate these results, we have employed the analysis of Ref. [1], and have used the values of CKM and non-perturbative parameters given in Table 1.

It is experimentally very challenging to reconstruct the  $\tau$  leptons, in particular in the environment of the LHC. Nevertheless, the LHCb collaboration has recently come up with the first experimental upper limits for the corresponding branching ratios [6]:

$$\bar{\mathcal{B}}(B_s \rightarrow \tau^+\tau^-) < 6.8 \times 10^{-3} \text{ (95\% C.L.)} \quad (77)$$



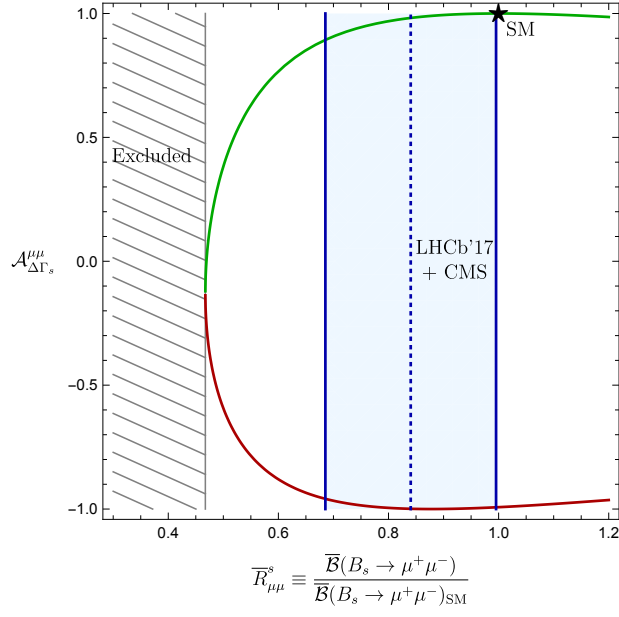


Figure 6: Correlation between  $\overline{R}_{\mu\mu}^s$  and  $\mathcal{A}_{\Delta\Gamma_s}^{\mu\mu}$  in the considered NP scenario. The green and red branches refer to the solutions I and II for  $A_{\mu\mu}^s$ , respectively.

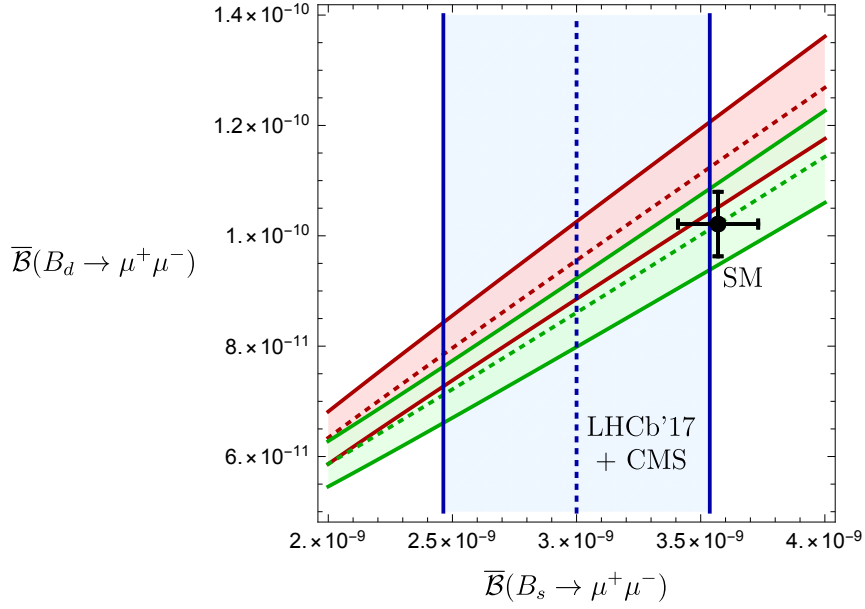


Figure 7: Correlation between the branching ratios  $\overline{\mathcal{B}}(B_d \rightarrow \mu^+\mu^-)$  and  $\overline{\mathcal{B}}(B_s \rightarrow \mu^+\mu^-)$  in the considered NP scenario. The green and red bands refer to the solutions I and II for  $A_{\mu\mu}^s$ , respectively, and correspond to  $1\sigma$  ranges.

$$\mathcal{B}(B_d \rightarrow \tau^+ \tau^-) < 2.1 \times 10^{-3} \text{ (95\% C.L.)}. \quad (78)$$

These results are in fact the first direct constraint for  $B_s^0 \rightarrow \tau^+ \tau^-$  and the world's best limit for  $B_d^0 \rightarrow \tau^+ \tau^-$ .

The SM predictions for  $\mathcal{A}_{\Delta\Gamma_s}^{\tau\tau}$  and  $\tau_{\tau\tau}^s$  take the same values as their  $B_s^0 \rightarrow \mu^+ \mu^-$  counterparts:

$$\mathcal{A}_{\Delta\Gamma_s}^{\tau\tau}|_{\text{SM}} = +1, \quad \tau_{\tau\tau}^s|_{\text{SM}} = \frac{\tau_{B_s}}{1 - y_s} = (1.61 \pm 0.06) \text{ ps}. \quad (79)$$

## 4.2 New Physics Benchmark Scenario

Let us now have a look at the NP effects for the  $B_{s,d}^0 \rightarrow \tau^+ \tau^-$  modes within the benchmark scenario introduced in Subsection 2.3. Here the coefficient  $C_P$  does not depend on the flavour of the final-state leptons. Consequently, using Eq. (31), we obtain

$$A_{\tau\tau}^s = \frac{m_\mu}{m_\tau} A_{\mu\mu}^s, \quad (80)$$

which allows us now to calculate  $P_{\tau\tau}^s$  and  $S_{\tau\tau}^s$ :

$$P_{\tau\tau}^s = 1 - \frac{m_\mu}{m_\tau} A_{\mu\mu}^s \quad (81)$$

$$S_{\tau\tau}^s = \sqrt{1 - 4 \frac{m_\tau^2}{M_{B_s}^2} \frac{m_\mu}{m_\tau} A_{\mu\mu}^s}, \quad (82)$$

yielding

$$\begin{aligned} \overline{R}_{\tau\tau}^s &= \frac{1 + y_s \cos \phi_s^{\text{NP}}}{1 + y_s} \left[ 1 - 2 \left( \frac{m_\mu}{m_\tau} \right) A_{\mu\mu}^s \right] \\ &+ \frac{2}{1 + y_s} \left[ 1 - 2 \frac{m_\tau^2}{M_{B_s}^2} \left( 1 - y_s \cos \phi_s^{\text{NP}} \right) \right] \left( \frac{m_\mu}{m_\tau} \right)^2 (A_{\mu\mu}^s)^2, \end{aligned} \quad (83)$$

and

$$\mathcal{A}_{\Delta\Gamma_s}^{\tau\tau} = \cos \phi_s^{\text{NP}} \left[ \frac{1 - 2 \left( \frac{m_\mu}{m_\tau} \right) A_{\mu\mu}^s + 4 \left( \frac{m_\mu}{M_{B_s}} \right)^2 (A_{\mu\mu}^s)^2}{1 - 2 \left( \frac{m_\mu}{m_\tau} \right) A_{\mu\mu}^s + 2 \left( \frac{m_\mu}{m_\tau} \right)^2 \left\{ 1 - 2 \left( \frac{m_\tau}{M_{B_s}} \right)^2 \right\} (A_{\mu\mu}^s)^2} \right]. \quad (84)$$

In this scenario, the NP effects in  $B_s^0 \rightarrow \tau^+ \tau^-$  are strongly suppressed with respect to  $B_s^0 \rightarrow \mu^+ \mu^-$  through the ratio of the muon and tau masses, which is given as follows [17]:

$$\frac{m_\mu}{m_\tau} = 0.059. \quad (85)$$

The twofold solution for  $A_{\mu\mu}^s$  in Eq. (69) gives the following results:

$$\overline{R}_{\tau\tau}^s|_{\text{I}} = 0.99 \pm 0.01, \quad \overline{R}_{\tau\tau}^s|_{\text{II}} = 0.89 \pm 0.01 \quad (86)$$

$$\mathcal{A}_{\Delta\Gamma_s}^{\tau\tau}|_{\text{I}} = 0.99995(24), \quad \mathcal{A}_{\Delta\Gamma_s}^{\tau\tau}|_{\text{II}} = 0.99570(89) \quad (87)$$

The impact of NP in the  $B_d^0 \rightarrow \tau^+ \tau^-$  decay is very similar to its  $B_s^0$  counterpart, with  $\overline{R}_{\tau\tau}^d$  taking the same values as in Eq. (86). Introducing a parameter  $U_{\tau\tau}^{ds}$  in analogy to Eq. (57), we obtain

$$U_{\tau\tau}^{ds}|_{\text{I}} = 1.000057(62), \quad U_{\tau\tau}^{ds}|_{\text{II}} = 1.00063(10). \quad (88)$$

In view of the challenges related to the reconstruction of the  $\tau$  leptons, the NP effects cannot be distinguished from the SM case, unless there is unexpected experimental progress.

## 5 The Decays $B_s^0 \rightarrow e^+e^-$ and $B_d^0 \rightarrow e^+e^-$

### 5.1 Observables

The most recent SM predictions for  $B_{s,d}^0 \rightarrow e^+e^-$  decays were given in Ref. [1]. Using the updated input parameters in Table 1, we obtain the following results:

$$\overline{\mathcal{B}}(B_s \rightarrow e^+e^-)_{\text{SM}} = (8.35 \pm 0.39) \times 10^{-14}. \quad (89)$$

$$\overline{\mathcal{B}}(B_d \rightarrow e^+e^-)_{\text{SM}} = (2.39 \pm 0.14) \times 10^{-15}. \quad (90)$$

The strong suppression of these branching ratios with respect to their  $B_{s,d}^0 \rightarrow \mu^+\mu^-$  counterparts arises from the helicity suppression due to the tiny electron mass, corresponding to an overall multiplicative factor  $m_e^2$  in the expressions for  $\mathcal{B}(B_{s,d} \rightarrow e^+e^-)$ . Within the SM, these decays appear to be out of reach from the experimental point of view, which seems to be the reason for the fact that these channels have so far essentially not played any role in the exploration of the quark-flavour sector.

Concerning the experimental picture, the CDF collaboration reported the following upper bounds (90% C.L.) back in 2009 [7]:

$$\overline{\mathcal{B}}(B_s \rightarrow e^+e^-) < 2.8 \times 10^{-7}, \quad (91)$$

$$\overline{\mathcal{B}}(B_d \rightarrow e^+e^-) < 8.3 \times 10^{-8}. \quad (92)$$

Consequently, any attempt to measure the SM branching ratios for the rare decays  $B_s^0 \rightarrow e^+e^-$  and  $B_d^0 \rightarrow e^+e^-$  would require a future improvement by nearly six orders of magnitude. The LHC experiments have not yet reported any searches for these modes.

### 5.2 New Physics Benchmark Scenario

Let us now consider the NP scenario introduced in Subsection 3.3. In this framework, we obtain the following relation:

$$A_{ee}^s = \frac{m_\mu}{m_e} A_{\mu\mu}^s. \quad (93)$$

While we got a suppression of the NP effects in the  $B_{s,d}^0 \rightarrow \tau^+\tau^-$  decays through the large  $\tau$  mass, see (80), we get now a huge enhancement thanks to the tiny electron mass [17]:

$$\frac{m_\mu}{m_e} = 206.77, \quad (94)$$

as the (pseudo)-scalar NP contributions lift the helicity suppression of the extremely small SM branching ratio. The relevant short-distance functions take the following form:

$$P_{ee}^s = 1 - \frac{m_\mu}{m_e} A_{\mu\mu}^s \quad (95)$$

$$S_{ee}^s = \sqrt{1 - 4 \frac{m_e^2}{M_{B_s}^2} \frac{m_\mu}{m_e} A_{\mu\mu}^s}, \quad (96)$$

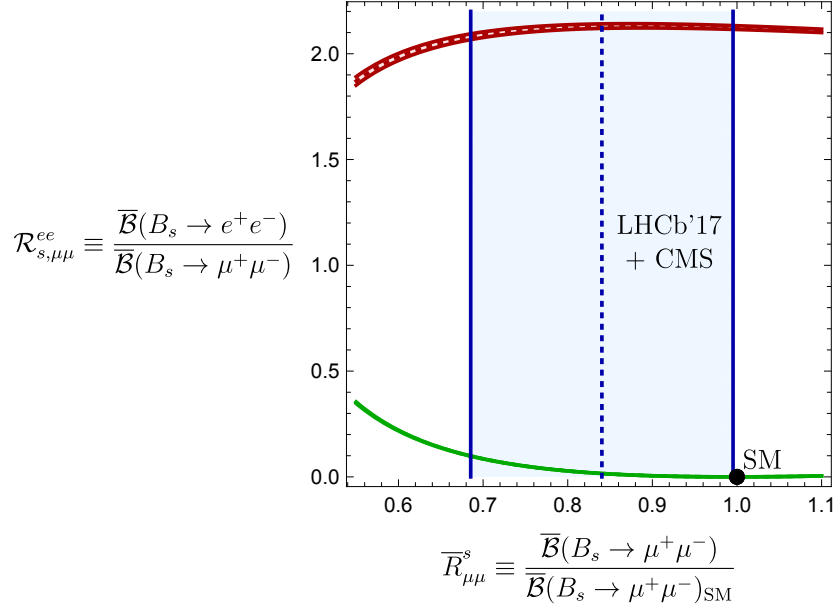


Figure 8: Correlation between the ratios  $\overline{\mathcal{B}}(B_s \rightarrow e^+e^-)/\overline{\mathcal{B}}(B_s \rightarrow \mu^+\mu^-)$  and  $\overline{R}_{\mu\mu}^s$  in our NP scenario. The green and red bands refer to the solutions I and II for the NP parameter  $A_{\mu\mu}^s$ , respectively, and correspond to  $1\sigma$  ranges.

yielding

$$\begin{aligned} \overline{R}_{ee}^s &= \frac{1 + y_s \cos \phi_s^{\text{NP}}}{1 + y_s} \left[ 1 - 2 \left( \frac{m_\mu}{m_e} \right) A_{\mu\mu}^s \right] \\ &\quad + \frac{2}{1 + y_s} \left[ 1 - 2 \frac{m_e^2}{M_{B_s}^2} \left( 1 - y_s \cos \phi_s^{\text{NP}} \right) \right] \left( \frac{m_\mu}{m_e} \right)^2 (A_{\mu\mu}^s)^2 \end{aligned} \quad (97)$$

and

$$\mathcal{A}_{\Delta\Gamma_s}^{ee} = \cos \phi_s^{\text{NP}} \left[ \frac{1 - 2 \left( \frac{m_\mu}{m_e} \right) A_{\mu\mu}^s + 4 \left( \frac{m_\mu}{M_{B_s}} \right)^2 (A_{\mu\mu}^s)^2}{1 - 2 \left( \frac{m_\mu}{m_e} \right) A_{\mu\mu}^s + 2 \left( \frac{m_\mu}{m_e} \right)^2 \left\{ 1 - 2 \left( \frac{m_e}{M_{B_s}} \right)^2 \right\} (A_{\mu\mu}^s)^2} \right]. \quad (98)$$

It is particularly interesting to consider the ratio between the  $B_s^0 \rightarrow e^+e^-$  and the  $B_s^0 \rightarrow \mu^+\mu^-$  branching ratios:

$$\begin{aligned} \mathcal{R}_{s,\mu\mu}^{ee} \equiv \frac{\overline{\mathcal{B}}(B_s \rightarrow e^+e^-)}{\overline{\mathcal{B}}(B_s \rightarrow \mu^+\mu^-)} &= \sqrt{\frac{1 - 4 \frac{m_e^2}{M_{B_s}^2}}{1 - 4 \frac{m_\mu^2}{M_{B_s}^2}}} \left[ \frac{2(A_{\mu\mu}^s)^2 \left\{ 1 - 2 \left( \frac{m_e}{M_{B_s}} \right)^2 y_- \right\} + y_+ \left( \frac{m_e}{m_\mu} \right) \left\{ \left( \frac{m_e}{m_\mu} \right) - 2A_{\mu\mu}^s \right\}}{2(A_{\mu\mu}^s)^2 \left\{ 1 - 2 \left( \frac{m_\mu}{M_{B_s}} \right)^2 y_- \right\} + y_+ (1 - 2A_{\mu\mu}^s)} \right] \\ &\approx \sqrt{\frac{1 - 4 \frac{m_e^2}{M_{B_s}^2}}{1 - 4 \frac{m_\mu^2}{M_{B_s}^2}}} \left[ \frac{2(A_{\mu\mu}^s)^2 \left\{ 1 - 2 \left( \frac{m_e}{M_{B_s}} \right)^2 \right\} - 2 \frac{m_e}{m_\mu} A_{\mu\mu}^s + \left( \frac{m_e}{m_\mu} \right)^2}{2(A_{\mu\mu}^s)^2 \left\{ 1 - 2 \left( \frac{m_\mu}{M_{B_s}} \right)^2 \right\} - 2A_{\mu\mu}^s + 1} \right], \end{aligned} \quad (99)$$

where we have, for simplicity, introduced

$$y_+ \equiv 1 + y_s \cos \phi_s^{\text{NP}}, \quad y_- \equiv 1 - y_s \cos \phi_s^{\text{NP}}. \quad (100)$$

In the last step of Eq. (99), we have neglected the phase  $\phi_s^{\text{NP}}$  together with the products involving  $y_s$ . As the decay constants and CKM matrix elements cancel in  $\mathcal{R}_{s,\mu\mu}^{ee}$ , this ratio

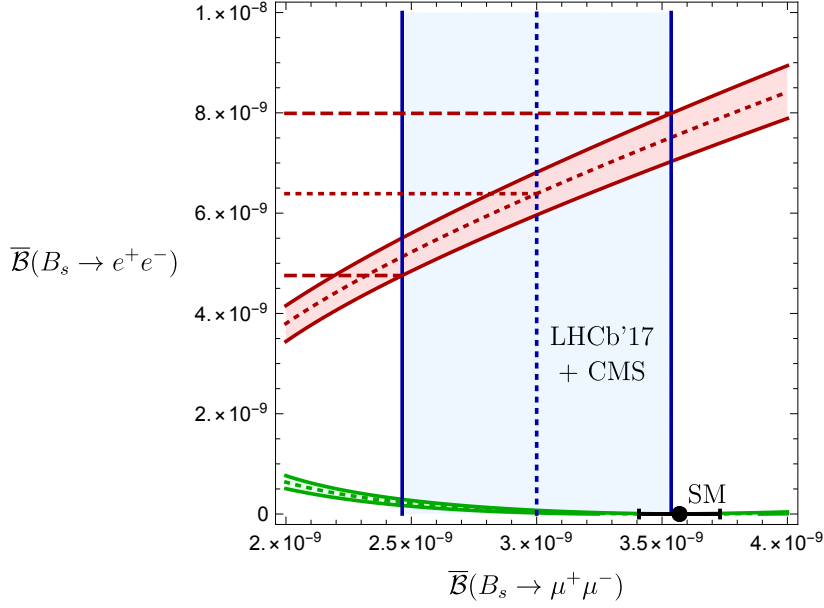


Figure 9: Correlation between  $\overline{\mathcal{B}}(B_s \rightarrow e^+e^-)$  and  $\overline{\mathcal{B}}(B_s \rightarrow \mu^+\mu^-)$  in the NP scenario. The green and red bands refer to the solutions I and II for the NP parameter  $A_{\mu\mu}^s$ , respectively, and correspond to  $1\sigma$  ranges.

is a particularly clean quantity from the theoretical point of view, and is not affected by the ratio  $f_s/f_d$  of fragmentation functions [34] from the experimental point of view.

Before calculating numerical ranges for  $\mathcal{R}_{s,\mu\mu}^{ee}$  with the help of Eq. (99), it is instructive to first get a qualitative understanding of this expression in the limits  $A_{\mu\mu}^s \rightarrow 0$  and  $A_{\mu\mu}^s \rightarrow 1$ , corresponding to the pattern of the twofold solution in Eq. (69). Taking also into account that the mass ratios  $m_e/m_\mu$ ,  $m_e/M_{B_s}$  and  $m_\mu/M_{B_s}$  are tiny, we find

$$\mathcal{R}_{s,\mu\mu}^{ee} = \left. \frac{\overline{\mathcal{B}}(B_s \rightarrow e^+e^-)}{\overline{\mathcal{B}}(B_s \rightarrow \mu^+\mu^-)} \right|_{A_{\mu\mu}^s \rightarrow 0} \longrightarrow \left( \frac{m_e}{m_\mu} \right)^2 - 2 \frac{m_e}{m_\mu} A_{\mu\mu}^s \sim \left( \frac{m_e}{m_\mu} \right)^2 \sim 0, \quad (101)$$

properly recovering the SM limit. On the other hand,

$$\begin{aligned} \mathcal{R}_{s,\mu\mu}^{ee} = \left. \frac{\overline{\mathcal{B}}(B_s \rightarrow e^+e^-)}{\overline{\mathcal{B}}(B_s \rightarrow \mu^+\mu^-)} \right|_{A_{\mu\mu}^s \rightarrow 1} &\longrightarrow 2(A_{\mu\mu}^s)^2 + \left( \frac{m_e}{m_\mu} \right)^2 \mathcal{O}(1) + \frac{m_e m_\mu}{M_{B_s}^2} \mathcal{O}(1) \\ &+ \left( \frac{m_\mu}{M_{B_s}} \right)^2 \mathcal{O}(1) + \left( \frac{m_e}{M_{B_s}} \right)^2 \mathcal{O}(1) \sim 2, \end{aligned} \quad (102)$$

which corresponds to a dramatic enhancement of  $\overline{\mathcal{B}}(B_s \rightarrow e^+e^-)$  by nearly five orders of magnitude with respect to the SM prediction.

Using the expression for  $\mathcal{R}_{s,\mu\mu}^{ee}$  in Eq. (99) and the twofold solution in Eq. (69) yields

$$\mathcal{R}_{s,\mu\mu}^{ee} \Big|_{\text{I}} = 0.02^{+0.04}_{-0.02}, \quad \mathcal{R}_{s,\mu\mu}^{ee} \Big|_{\text{II}} = 2.13 \pm 0.02. \quad (103)$$

We illustrate the correlation between  $\mathcal{R}_{s,\mu\mu}^{ee}$  and  $\overline{R}_{\mu\mu}^s$  in Fig. 8. It is remarkable to see the tiny uncertainty of the former ratio, which is due to the theoretical cleanliness of this observable discussed above.

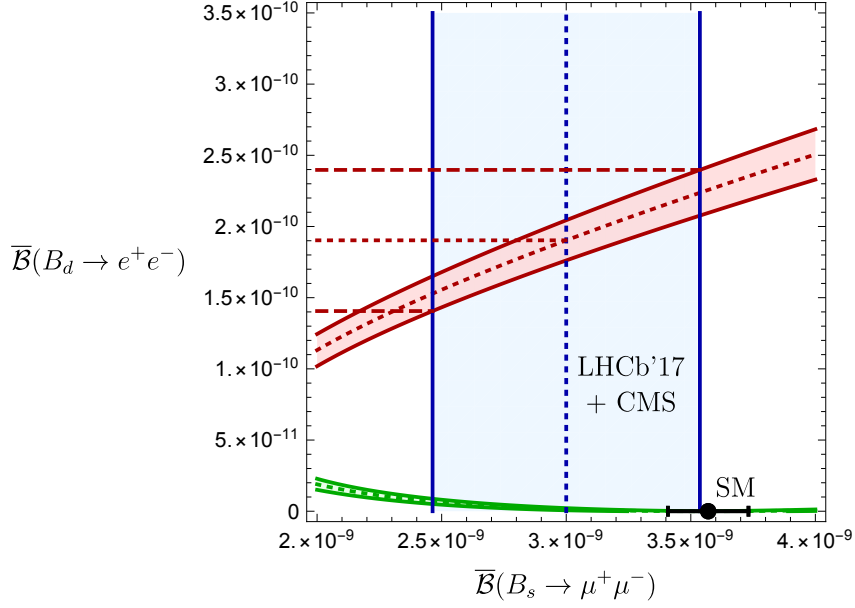


Figure 10: Correlation between  $\bar{\mathcal{B}}(B_d \rightarrow e^+e^-)$  and  $\bar{\mathcal{B}}(B_s \rightarrow \mu^+\mu^-)$  in NP scenario. The green and red bands refer to the solutions I and II for the NP parameter  $A_{\mu\mu}^s$ , respectively, and correspond to  $1\sigma$  ranges.

In the case of the branching ratio of the  $B_s^0 \rightarrow e^+e^-$  channel, we obtain uncertainties from the  $f_{B_s}$  decay constant, CKM factors and the  $B_s$  lifetime  $\tau_{B_s}$ . The results in Eq. (103) correspond to the following results:

$$\bar{\mathcal{B}}(B_s \rightarrow e^+e^-)|_{\text{I}} = (4.8 \pm 10.5) \times 10^{-11}, \quad \bar{\mathcal{B}}(B_s \rightarrow e^+e^-)|_{\text{II}} = (6.39 \pm 1.25) \times 10^{-9}, \quad (104)$$

with

$$\bar{R}_{ee}^s|_{\text{I}} = 571.8 \times [1.0_{-1.0}^{+2.2}], \quad \bar{R}_{ee}^s|_{\text{II}} = 76483.3 \times [1.0 \pm 0.2], \quad (105)$$

showing an impressive lift of the helicity suppression with respect to the SM value in Eq. (89). The correlation between  $\bar{\mathcal{B}}(B_s \rightarrow e^+e^-)$  and  $\bar{\mathcal{B}}(B_s \rightarrow \mu^+\mu^-)$  is shown in Fig. 9. We complement our analysis of the  $B_s^0 \rightarrow e^+e^-$  channel by calculating

$$\mathcal{A}_{\Delta\Gamma_s}^{ee}|_{\text{I}} = -(5.7 \pm 6.3) \times 10^{-2}, \quad \mathcal{A}_{\Delta\Gamma_s}^{ee}|_{\text{II}} = -(5.0 \pm 0.5) \times 10^{-3}. \quad (106)$$

The pattern of the NP effects in  $B_d^0 \rightarrow e^+e^-$  is very similar to the situation in its  $B_s^0$  counterpart. We show the correlation between the branching ratios  $\bar{\mathcal{B}}(B_d \rightarrow e^+e^-)$  and  $\bar{\mathcal{B}}(B_s \rightarrow \mu^+\mu^-)$  in Fig. 10, and obtain the following results for the current measurement of the latter branching ratio:

$$\bar{\mathcal{B}}(B_d \rightarrow e^+e^-)|_{\text{I}} = (1.4 \pm 3.1) \times 10^{-12}, \quad \bar{\mathcal{B}}(B_d \rightarrow e^+e^-)|_{\text{II}} = (1.9 \pm 0.4) \times 10^{-10}. \quad (107)$$

Introducing a parameter  $U_{ee}^{ds}$  in analogy to Eq. (57), we obtain

$$U_{ee}^{ds}|_{\text{I}} = 0.9886 \pm 0.0015, \quad U_{ee}^{ds}|_{\text{II}} = 0.9889 \pm 0.0014. \quad (108)$$

The strongly constrained pattern of the NP effects in the  $B_{s,d}^0 \rightarrow e^+e^-$  channels and their correlation with the  $B_{s,d}^0 \rightarrow \mu^+\mu^-$  observables is characteristic for the considered NP model, thereby offering an excellent playground for the future data taking.

## 6 Conclusions

Leptonic rare decays of  $B_s^0$  and  $B_d^0$  mesons play an outstanding role for testing the SM. The main actors have so far been the  $B_s^0 \rightarrow \mu^+\mu^-$  and  $B_d^0 \rightarrow \mu^+\mu^-$  modes, where the former channel is now well established in the LHC data and first signals for the latter channel were reported. Very recently, LHCb has presented the first measurement of the effective lifetime of  $B_s^0 \rightarrow \mu^+\mu^-$ , and upper bounds for the  $B_s^0 \rightarrow \tau^+\tau^-$  and  $B_d^0 \rightarrow \tau^+\tau^-$  modes. The experimental constraint for  $\mathcal{B}(B_s \rightarrow e^+e^-)$  is six orders of magnitude above the SM prediction, and was obtained by CDF in 2009.

In this paper, we have given a state-of-the-art discussion of the interpretation of the  $B_{s,d}^0 \rightarrow \mu^+\mu^-$  data. However, the main focus was on the decays with tau leptons and muons in the final state, addressing the question of how much space for NP effects is left by the current data, in particular the observation of  $B_s^0 \rightarrow \mu^+\mu^-$ . In order to explore this issue, which is in general very involved, we have considered a NP scenario as a benchmark which is characterized by having heavy new particles and the feature of MFV. In particular, it includes the MFV SUSY model, satisfying also the current constraints on direct searches for SUSY particles at the ATLAS and CMS experiments. Using the measured  $B_s^0 \rightarrow \mu^+\mu^-$  branching ratio, we obtain a twofold solution for a NP parameter  $A_{\mu\mu}^s$  characterizing the specific model.

We find that the NP effects are strongly suppressed by the mass ratio  $m_\mu/m_\tau$  in the  $B_{s,d}^0 \rightarrow \tau^+\tau^-$  decays, thereby resulting in a picture which is essentially as in the SM. On the other hand, the NP effects are amplified in the  $B_s^0 \rightarrow e^+e^-$  channel due to the mass ratio  $m_\mu/m_e$ . In this case, the helicity suppression is lifted by new (pseudo)-scalar contributions, while the branching ratio of  $B_s^0 \rightarrow \mu^+\mu^-$  stays close to its SM value. The solution of  $A_{\mu\mu}^s$  with  $\mathcal{A}_{\Delta\Gamma_s}^{\mu\mu} \sim -1$  (taking a sign opposite to the SM case) gives a value of the  $B_s^0 \rightarrow e^+e^-$  branching ratio about *twice* as large as the  $B_s^0 \rightarrow \mu^+\mu^-$  branching ratio, which is a factor of about 50 below the CDF limit. The ratio  $\mathcal{R}_{s,\mu\mu}^{ee}$  of the  $B_s^0 \rightarrow e^+e^-$  and  $B_s^0 \rightarrow \mu^+\mu^-$  branching ratios is a particularly clean quantity, having also advantages from the experimental point of view.

Due to the helicity structure of possible NP contributions,  $B_s^0 \rightarrow e^+e^-$  is in general a very sensitive probe of physics beyond the SM with new (pseudo)-scalar contributions. As this decay has essentially not received any attention since the CDF analysis from 2009, it would be most interesting to search for  $B_s^0 \rightarrow e^+e^-$  in the LHC data, with the possibility of finding a signal which would give us unambiguous evidence for New Physics.

In order to get the full picture, also  $B_s^0 \rightarrow \tau^+\tau^-$  and the corresponding  $B_d^0$  modes should receive full attention at the LHC and the future Belle II experiments. We are excited to see new results – in particular searches for the  $B_{s,d}^0 \rightarrow e^+e^-$  decays – which may eventually open a wide window to the physics beyond the Standard Model.

## Acknowledgements

This research has been supported by the Netherlands Foundation for Fundamental Research of Matter (FOM) programme 156, “Higgs as Probe and Portal”, and by the National Organisation for Scientific Research (NWO).

## References

- [1] C. Bobeth, M. Gorbahn, T. Hermann, M. Misiak, E. Stamou and M. Steinhauser, Phys. Rev. Lett. **112** (2014) 101801 doi:10.1103/PhysRevLett.112.101801 [arXiv:1311.0903 [hep-ph]].
- [2] G. Borissov, R. Fleischer and M. H. Schune, Ann. Rev. Nucl. Part. Sci. **63** (2013) 205 doi:10.1146/annurev-nucl-102912-144527 [arXiv:1303.5575 [hep-ph]].
- [3] V. Khachatryan *et al.* [CMS and LHCb Collaborations], Nature **522** (2015) 68 doi:10.1038/nature14474 [arXiv:1411.4413 [hep-ex]].
- [4] K. De Bruyn, R. Fleischer, R. Knegjens, P. Koppenburg, M. Merk, A. Pellegrino and N. Tuning, Phys. Rev. Lett. **109** (2012) 041801 doi:10.1103/PhysRevLett.109.041801 [arXiv:1204.1737 [hep-ph]].
- [5] R. Aaij *et al.* [LHCb Collaboration], arXiv:1703.05747 [hep-ex].
- [6] R. Aaij *et al.* [LHCb Collaboration], arXiv:1703.02508 [hep-ex].
- [7] T. Aaltonen *et al.* [CDF Collaboration], Phys. Rev. Lett. **102** (2009) 201801 doi:10.1103/PhysRevLett.102.201801 [arXiv:0901.3803 [hep-ex]].
- [8] W. Altmannshofer, C. Niehoff and D. M. Straub, arXiv:1702.05498 [hep-ph].
- [9] G. D'Ambrosio, G. F. Giudice, G. Isidori and A. Strumia, Nucl. Phys. B **645** (2002) 155 doi:10.1016/S0550-3213(02)00836-2 [hep-ph/0207036].
- [10] I. Dunietz, R. Fleischer and U. Nierste, Phys. Rev. D **63** (2001) 114015 doi:10.1103/PhysRevD.63.114015 [hep-ph/0012219].
- [11] A. J. Buras, R. Fleischer, J. Girrbach and R. Knegjens, JHEP **1307** (2013) 77 doi:10.1007/JHEP07(2013)077 [arXiv:1303.3820 [hep-ph]].
- [12] Y. Amhis *et al.* [Heavy Flavor Averaging Group], arXiv:1612.07233 [hep-ex] and online update at <http://www.slac.stanford.edu/xorg/hfag/>.
- [13] K. De Bruyn, R. Fleischer, R. Knegjens, P. Koppenburg, M. Merk and N. Tuning, Phys. Rev. D **86** (2012) 014027 doi:10.1103/PhysRevD.86.014027 [arXiv:1204.1735 [hep-ph]].
- [14] K. De Bruyn and R. Fleischer, JHEP **1503** (2015) 145 doi:10.1007/JHEP03(2015)145 [arXiv:1412.6834 [hep-ph]].
- [15] CKMfitter Group Collaboration, <http://ckmfitter.in2p3.fr>
- [16] R. Alonso, B. Grinstein and J. Martin Camalich, Phys. Rev. Lett. **113** (2014) 241802 doi:10.1103/PhysRevLett.113.241802 [arXiv:1407.7044 [hep-ph]].
- [17] P. J. Mohr, D. B. Newell and B. N. Taylor, Rev. Mod. Phys. **88** (2016) no.3, 035009 doi: 10.1103/RevModPhys.88.035009 [physics.atom-ph/1507.07956] <http://physics.nist.gov/cuu/Constants/>.



- [18] 2016 Review of Particle Physics. C. Patrignani et al.(Particle Data Group), Chin. Phys. C, 40 (2016) 100001.
- [19] S. Aoki et al., Review of lattice results concerning low-energy particle physics, [hep-lat/1607.00299].
- [20] S. Chatrchyan *et al.* [CMS Collaboration], Phys. Rev. Lett. **111** (2013) 101804 doi:10.1103/PhysRevLett.111.101804 [arXiv:1307.5025 [hep-ex]].
- [21] M. Aaboud *et al.* [ATLAS Collaboration], Eur. Phys. J. C **76** (2016) no.9, 513 doi:10.1140/epjc/s10052-016-4338-8 [arXiv:1604.04263 [hep-ex]].
- [22] A. J. Buras and R. Fleischer, Adv. Ser. Direct. High Energy Phys. **15** (1998) 65 [hep-ph/9704376].
- [23] L. Wolfenstein, Phys. Rev. Lett. **51** (1983) 1945.
- [24] A. J. Buras, M. E. Lautenbacher and G. Ostermaier, Phys. Rev. D **50** (1994) 3433 doi:10.1103/PhysRevD.50.3433 [hep-ph/9403384].
- [25] M. Gronau and D. Wyler, Phys. Lett. B **265** (1991) 172. doi:10.1016/0370-2693(91)90034-N
- [26] D. Atwood, I. Dunietz and A. Soni, Phys. Rev. Lett. **78** (1997) 3257 doi:10.1103/PhysRevLett.78.3257 [hep-ph/9612433]; Phys. Rev. D **63** (2001) 036005 doi:10.1103/PhysRevD.63.036005 [hep-ph/0008090].
- [27] R. Fleischer and S. Ricciardi, proceedings of the 6th International Workshop on the CKM Unitarity Triangle (CKM 2010) [arXiv:1104.4029 [hep-ph]].
- [28] T. Abe *et al.* [Belle-II Collaboration], arXiv:1011.0352 [physics.ins-det].
- [29] R. Aaij *et al.* [LHCb Collaboration], Eur. Phys. J. C **73** (2013) 2373 doi:10.1140/epjc/s10052-013-2373-2 [arXiv:1208.3355 [hep-ex]].
- [30] A. Bevan *et al.*, arXiv:1411.7233 [hep-ph]; for updates, see <http://www.utfit.org>.
- [31] M. Blanke and A. J. Buras, Eur. Phys. J. C **76** (2016) no. 4, 197 doi:10.1140/epjc/s10052-016-4044-6 [arXiv:1602.04020 [hep-ph]].
- [32] A. J. Buras, Phys. Lett. B **566** (2003) 115 doi:10.1016/S0370-2693(03)00561-6 [hep-ph/0303060].
- [33] H. E. Logan and U. Nierste, Nucl. Phys. B **586** (2000) 39 doi:10.1016/S0550-3213(00)00417-X [hep-ph/0004139].
- [34] R. Fleischer, N. Serra and N. Tuning, Phys. Rev. D **82** (2010) 034038 doi:10.1103/PhysRevD.82.034038 [arXiv:1004.3982 [hep-ph]].